

# DYNAMIC MR IMAGE AND FIELDMAP JOINT RECONSTRUCTION ACCOUNTING FOR THROUGH-PLANE FIELDMAP GRADIENTS

Antonios Matakos and Jeffrey A. Fessler

Department of Electrical Engineering and Computer Science  
The University of Michigan  
1301 Beal Avenue, Ann Arbor, MI 48109-2122

## ABSTRACT

In susceptibility-weighted MRI, ignoring the magnetic field inhomogeneity can lead to severe reconstruction artifacts. Correcting for the effects of magnetic field inhomogeneity requires accurate fieldmaps. Especially in functional MRI, dynamic updates are desirable, since the fieldmap may change in time. Also, susceptibility effects that induce field inhomogeneity often have non-zero through-plane gradients, which, if uncorrected, can cause signal loss in the reconstructed images. Most image reconstruction methods that compensate for field inhomogeneity, even using dynamic fieldmap updates, ignore through-plane fieldmap gradients. This work proposes a computationally efficient, model based iterative method for joint reconstruction of image and dynamic fieldmap that accounts for the through-plane gradients of the field inhomogeneity. The proposed method allows for efficient reconstruction by applying fast approximations that allow the use of the conjugate gradient algorithm along with FFTs.

**Index Terms**— Through-plane gradients, dynamic field map estimation, iterative reconstruction.

## 1. INTRODUCTION

In functional MRI a series of dynamic images is reconstructed and to satisfy the need for high temporal resolution, fast single-shot acquisitions are commonly used. Also these acquisition usually have late echo-times to ensure good BOLD contrast. These characteristics of susceptibility-weighted MR imaging lead to increased sensitivity to magnetic field inhomogeneities. Correcting for these effects requires accurate inhomogeneity fieldmaps and since the fieldmap may change in time, dynamic updates are desirable. This motivated the development of methods that can jointly reconstruct undistorted images and undistorted dynamic fieldmaps [1], [2] and [3].

Most methods correcting for field inhomogeneity, even the model-based iterative ones, treat the inhomogeneity within each voxel as being a constant. However, susceptibility effects usually cause nonzero through-plane gradients that lead to spin dephasing across the slice within each voxel. Ignoring through-plane gradients can cause signal loss in the reconstructed images, especially in functional MR imaging where acquisitions with long readouts and late echo-times are used. To correct for the through-plane gradient effects, a fast, iterative reconstruction method is proposed in [4]. That method assumed that the through-plane gradients are known, so it cannot handle dynamic fieldmap changes.

Motivated by [2], this work proposes a computationally efficient, model based, iterative method that jointly reconstructs images and

dynamic fieldmaps, accounting for through-plane gradient effects. The proposed algorithm uses the signal model presented in [4] and applies the fast approximations introduced in [5]. Finally to improve the efficiency of the reconstruction algorithm, similarly to [6], a linearization technique for fieldmap estimation is used, that allows the use of the CG algorithm.

## 2. THEORY

To correct for through-plane gradient effects, we need a signal model that accounts for the slice profile and the through plane gradients of the field inhomogeneity. Assuming a total of  $J$  slices and parallel imaging with  $n_c$  coils, a reasonable model for the signal in slice selective MRI is:

$$s_{j,i}(t) = \iiint h(z - z_j) c_i(x, y, z) f(x, y, z) e^{-i\omega(x, y, z)t} e^{-i2\pi(k_X(t)x + k_Y(t)y)} dx dy dz, \quad (1)$$

for  $i = 1, \dots, n_c$  and  $j = 1, \dots, J$ ,

where  $h(z)$  is the (known) slice-selection profile,  $z_j$  is the axial center of the  $j$ th slice,  $f(x, y, z)$  is the (unknown) object,  $\omega(x, y, z)$  is the fieldmap,  $c_i(x, y, z)$  is the coil sensitivity and  $k(t) \triangleq (k_X(t), k_Y(t))$  is the k-space trajectory. We assume that the object  $f$  and the fieldmap  $\omega$  are static during a single-shot readout.

The model in (1) is equivalent to that proposed in [4] and using the same assumptions and approximations introduced therein, the discretized signal equation is expressed as:

$$s_{j,i}(t) = \Phi(k(t)) \sum_{n=0}^{N-1} H(g_{j,n}t) c_{j,i,n} f_{j,n} e^{-i\omega_{j,n}t} e^{-i2\pi k(t) \cdot r_n}, \quad (2)$$

where  $\Phi(k(t))$  is the Fourier transform of the basis function,  $H(\cdot)$  is the Fourier transform of the slice profile and  $g$  is the through-plane gradient, determined from the fieldmap using central differences, *i.e.*,  $g_{j,n} \triangleq \frac{\omega_{j+1,n} - \omega_{j-1,n}}{4\pi\Delta z}$ .

The model is non-linear in  $\omega$  (2). To avoid using a computationally demanding GD method as in [1], we follow [6] and linearize the signal equation by approximating the term  $H(g_j t) e^{-i\omega_j t}$  using first-order Taylor series expansion around a carefully chosen reference  $\tilde{\omega}$ . The suitability of the linearization depends on having a reasonable initial fieldmap estimate  $\tilde{\omega}$ ; typically  $\tilde{\omega}$  is obtained from a pre-scan or from the previous dynamic frame. This leads to the following

---

This work is supported in part by NIH grant P01CA87634.

approximation:

$$\begin{aligned}
H(\check{g}_j t) e^{-i\check{\omega}_j t} &\approx H(\check{g}_j t) e^{-i\check{\omega}_j t} - it H(\check{g}_j t) e^{-i\check{\omega}_j t} (\omega_j - \check{\omega}_j) \\
&\quad - \frac{t}{4\pi\Delta z} H'(\check{g}_j t) e^{-i\check{\omega}_j t} (\omega_{j-1} - \check{\omega}_{j-1}) \\
&\quad + \frac{t}{4\pi\Delta z} H'(\check{g}_j t) e^{-i\check{\omega}_j t} (\omega_{j+1} - \check{\omega}_{j+1}), \quad (3)
\end{aligned}$$

where  $H'(u) \triangleq \frac{dH(u)}{du}$  and  $\check{g}_j \triangleq \frac{\check{\omega}_{j+1,n} - \check{\omega}_{j-1,n}}{4\pi\Delta z}$ .

MRI measurements are noisy samples of the signal. Using the approximation (3) in the signal equation (2), the measurement vectors  $y_{j,i}$  for each slice and each coil can be expressed in matrix vector form as:

$$\begin{aligned}
y_{j,i} &= A(\check{\omega}_j, \check{g}_j, c_{j,i}) f_j + B(\check{\omega}_j, \check{g}_j, f_j, c_{j,i}) (\omega_j - \check{\omega}_j) \\
&\quad + D(\check{\omega}_j, \check{g}_j, f_j, c_{j,i}) (\omega_{j-1} - \check{\omega}_{j-1}) \\
&\quad - D(\check{\omega}_j, \check{g}_j, f_j, c_{j,i}) (\omega_{j+1} - \check{\omega}_{j+1}) + \varepsilon_{j,i}, \quad (4)
\end{aligned}$$

where  $f_j \triangleq (f_{j,1}, \dots, f_{j,N})$ ,  $\omega_j \triangleq (\omega_{j,1}, \dots, \omega_{j,N})$  and  $c_{j,i} \triangleq (c_{j,i,1}, \dots, c_{j,i,N})$  are the discretized object, fieldmap and sensitivity map respectively, and the elements of the  $M \times N$  system matrices  $A(\check{\omega}_j, \check{g}_j, c_{j,i})$ ,  $B(\check{\omega}_j, \check{g}_j, f_j, c_{j,i})$  and  $D(\check{\omega}_j, \check{g}_j, f_j, c_{j,i})$  are:

$$\begin{aligned}
a(\check{\omega}_j, \check{g}_j, c_{j,i})_{m,n} &= H(\check{g}_j, n t_m) w(\check{\omega}_j, \check{g}_j, c_{j,i})_{m,n}, \\
b(\check{\omega}_j, \check{g}_j, f_j, c_{j,i})_{m,n} &= -it_m a(\check{\omega}_j, \check{g}_j, c_{j,i})_{m,n} f_{j,n}, \quad (5) \\
d(\check{\omega}_j, \check{g}_j, f_j, c_{j,i})_{m,n} &= -\frac{t_m}{4\pi\Delta z} H'(\check{g}_j, n t_m) w(\check{\omega}_j, \check{g}_j, c_{j,i})_{m,n} f_{j,n}, \\
w(\check{\omega}_j, \check{g}_j, c_{j,i})_{m,n} &\triangleq \Phi(k(t_m)) e^{-i\check{\omega}_j, n t_m} e^{-i2\pi k(t_m) \cdot r_n} c_{j,i,n}.
\end{aligned}$$

When one ignores through-plane gradients (assuming  $g_j = 0$ ), the measurement model in (4) is equivalent to the approach described in [2] and the joint reconstruction problem can be solved with the fast iterative algorithm described therein. The presence of the  $H(\check{g}_j t)$  and  $H'(\check{g}_j t)$  terms in (5) prohibits the direct application of those fast methods. To solve this problem, we used the following approximations based on the histogram PCA basis expansion approach described in [5]:

$$\begin{aligned}
H(\check{g}_j, n t_m) e^{-i\check{\omega}_j, n t_m} &\approx \sum_{l=1}^L p_{j,m,l} q_{j,l,n}, \\
H'(\check{g}_j, n t_m) e^{-i\check{\omega}_j, n t_m} &\approx \sum_{l=1}^L u_{j,m,l} v_{j,l,n}. \quad (6)
\end{aligned}$$

Using the approximation in (6) into the expressions in (5), allows the evaluation of the forward model or its adjoint using  $L$  NUFFT calls.

The measurement vector for each slice  $y_j$  is given by stacking the measurement vectors  $y_{j,i}$  for each coil and the overall  $n_c M \times N$  system matrices are given by stacking the system matrices for each coil. Hence, the overall measurement model for each slice in matrix-vector form can be written as:

$$\begin{aligned}
y_j &= A_C(\check{\omega}_j, \check{g}_j) f_j + B_C(\check{\omega}_j, \check{g}_j, f_j) (\omega_j - \check{\omega}_j) \\
&\quad + D_C(\check{\omega}_j, \check{g}_j, f_j) (\omega_{j-1} - \check{\omega}_{j-1}) \\
&\quad - D_C(\check{\omega}_j, \check{g}_j, f_j) (\omega_{j+1} - \check{\omega}_{j+1}) + \varepsilon_j. \quad (7)
\end{aligned}$$

In (7) there is coupling between adjacent slices of the fieldmap. It should be beneficial to account for this coupling when reconstructing, by estimating all the slices at once and treating the problem as a 3D reconstruction instead of a sequential 2D reconstruction. With this in mind, we write the measurement model as:

$$y = A_J(\check{\omega}) f + B_J(\check{\omega}, f) (\omega - \check{\omega}) + \varepsilon, \quad (8)$$

where the vectors  $y$ ,  $f$  and  $\omega$  are created by stacking the individual slice vectors  $y_j$ ,  $f_j$  and  $\omega_j$  respectively and the  $n_c JM \times JN$  matrices  $A_J$  and  $B_J$  are defined as follows:<sup>1</sup>

$$\begin{aligned}
A_J &= \begin{bmatrix} A_{C,1} & 0 & \cdots & 0 \\ 0 & A_{C,2} & \ddots & \vdots \\ \vdots & \ddots & \ddots & 0 \\ 0 & \cdots & 0 & A_{C,J} \end{bmatrix} \quad (9) \\
B_J &= \begin{bmatrix} B_1 + 2D_1 & -2D_1 & 0 & \cdots & 0 \\ D_2 & B_2 & -D_2 & \ddots & \vdots \\ 0 & \ddots & \ddots & \ddots & 0 \\ \vdots & \ddots & D_{J-1} & B_{J-1} & -D_{J-1} \\ 0 & \cdots & 0 & 2D_J & B_J - 2D_J \end{bmatrix}
\end{aligned}$$

To estimate the image and fieldmap accounting for noise statistics, we minimize the following regularized least squares cost function:

$$\begin{aligned}
\Psi(f, \omega) &= \frac{1}{2} \|y - A_J(\check{\omega}) f - B_J(\check{\omega}, f) (\omega - \check{\omega})\|^2 \\
&\quad + \beta_1 R_1(f) + \beta_2 R_2(\omega), \quad (10)
\end{aligned}$$

where  $R_1(f)$  and  $R_2(\omega)$  are regularization terms. The fieldmap is smooth, both in the in-plane and through-plane directions, so we use a quadratic regularization penalty  $R_2(\omega) \triangleq \frac{1}{2} \|C_2 \omega\|^2$ , where  $C_2$  is a matrix of second-order differences along all three directions ( $x$ ,  $y$ ,  $z$ ). For the image  $f$ , an edge-preserving regularizer could be used, but since fMRI images are often smoothed for data analysis, we also used a quadratic regularizer  $R_1(f) \triangleq \frac{1}{2} \|C_1 f\|^2$  here, where  $C_1$  is a matrix of second-order differences along the  $x$  and  $y$  directions.

We minimize the cost function (10) by alternating between updating the image and the fieldmap. In each step of the minimization process a new update is found for the image and then for the fieldmap and the process is repeated until convergence. For the  $k$ th step in the alternating minimization scheme, the image update is:

$$\hat{f}^k = \underset{f}{\operatorname{argmin}} \frac{1}{2} \|y - A_J(\hat{\omega}^{k-1}) f\|^2 + \beta_1 R(f) \quad (11)$$

and the fieldmap update uses the most recent image:

$$\hat{\omega}^k = \underset{\omega}{\operatorname{argmin}} \frac{1}{2} \|\hat{y}^k - B_J(\hat{\omega}^{k-1}, \hat{f}^k) \omega\|^2 + \beta_2 R(\omega), \quad (12)$$

where

$$\hat{y}^k \triangleq y - A_J(\hat{\omega}^{k-1}) \hat{f}^k + B_J(\hat{\omega}^{k-1}, \hat{f}^k) \hat{\omega}^{k-1}.$$

In both (11) and (12) the minimizers are found using the CG-Toeplitz method [5] which is reasonably computationally efficient. For EPI trajectories standard FFTs can be used instead of the NUFFT.

### 3. MATERIALS AND METHODS

The proposed method is applicable with any k-space trajectory, although the results depend on the trajectory choice. As proposed in [2], the choice of an ‘‘interleaved’’, single-shot EPI trajectory,

<sup>1</sup>In (9), the dependency of  $A_C$ ,  $B_C$  and  $D_C$  on  $\omega_j$ ,  $g_j$  and  $f_j$  is only expressed through the subscript  $j = 1, \dots, J$  due to lack of space.

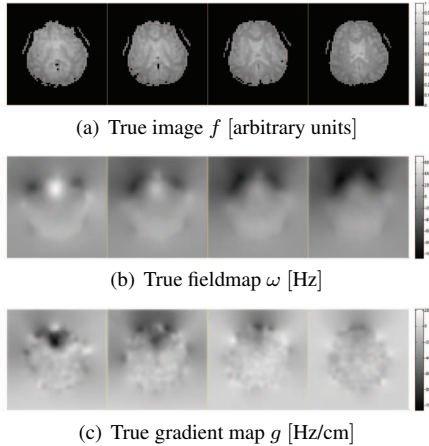


**Fig. 1.** True image, fieldmap and gradient map for 4 out of 20 slices. Slices 3, 8, 13 and 18 are shown from left to right.

along with sensitivity encoding, allows for successful joint reconstruction of image and fieldmap. Thus, we used this type of trajectory to assess the proposed method. The trajectory parameters are FOV = 24 cm, matrix size =  $64 \times 64$ , readout time = 46 ms and two echo-times at  $T_{E1} = 18$  ms and  $T_{E2} = 42$  ms. For parallel imaging in simulations, a four coil setting with smooth B1 maps was used.

For the simulation experiments human brain data (both images and fieldmaps) were used, acquired with the method described in [7]. The scans were  $64 \times 64$  by 20 slices, with 24 cm transaxial FOV and 2 cm axial FOV, resulting in slice spacing of 1 mm. For the slice selection, a rectangular profile was used with 4 mm width. The magnitude images and the corresponding fieldmaps of 4 slices are shown in Figs. 1(a) and 1(b). The fieldmap gradients, shown in Fig. 1(c), were estimated from the fieldmaps using central differences.

The experiments were performed with simulated data, created using the exact system model (2), to which noise was added to make a 30dB and 50dB data SNR. We used an iteratively reconstructed image, uncorrected for field inhomogeneities, as the initial estimate  $f_0$ , and we created the initial estimate  $\omega_0$  with the standard phase difference method from two images using iterative CG reconstruction uncorrected for field inhomogeneities. The images were acquired with 2-shot EPI trajectories, at 40dB data SNR. Each shot of the EPI had a 22.5 ms readout time and the echo-times were  $T_{E1} = 12.3$  ms for the first acquisition and  $T_{E2} = 14.3$  ms for the second, resulting in a  $\Delta T_E = 2$  ms echo-time difference. The resulting distorted fieldmaps were smoothed with a Gaussian filter to suppress the noise. The RMS and maximum error of the initial fieldmap can be seen in Table 1. As seen in the results section, the joint reconstruction method works well when the initial fieldmap is within 10 Hz from the true fieldmap, although a more thorough investigation of these limits is required. Nevertheless, the expected variations of the fieldmap in an fMRI study, as presented in [1], are well within this range.

To further evaluate the quality of the joint reconstruction, an oracle image estimate was reconstructed with our method using the true fieldmap (Fig. 2(a)) and an oracle fieldmap estimate was reconstructed with our method using the true image (Fig. 2(b)). These oracle estimates provide an upper bound on the accuracy of the proposed joint reconstruction method.

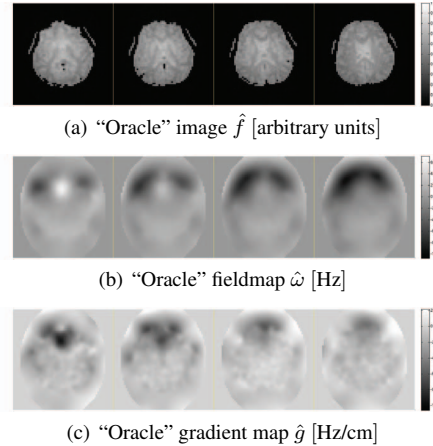


**Fig. 2.** Oracle image, fieldmap and gradient map for 4 out of 20 slices. Slices 3, 8, 13 and 18 are shown from left to right.

The regularization parameters  $\beta_1$  and  $\beta_2$  in (11) and (12) were chosen to achieve a specific spatial resolution [8]. For the image we chose  $\beta_1$  so that the FWHM of the PSF was 1.1 pixels at 50dB SNR and 1.2 pixels at 30dB SNR. For the fieldmap we chose  $\beta_2$  so that the FWHM of the PSF was 1.2 voxels (since 3D regularization is applied) for both SNRs.

To jointly estimate the image and fieldmap we alternated 20 times between updating the image and then updating the fieldmap. In each update we used 15 iterations of the CG method. The necessary matrix-vector multiplications in each CG iteration were performed with the Toeplitz, histogram PCA method of [5], with  $L = 9$  basis functions. The CG-Toeplitz method requires updates of the basis and coefficients in each alternating step, which can be a computational bottleneck, since calculating a new basis requires to perform a SVD. To alleviate this problem, the basis functions were precalculated at the beginning of the study and only the coefficients were updated in each alteration. Given reasonable initial estimates, this is a valid simplification, because the nature of the image and the fieldmap does not change dramatically with each update. The computational cost per iteration is in the order of  $O(N \log N)$  and it requires roughly three times more computations per iteration compared to the method in [6].

#### 4. SIMULATION RESULTS

Fig. 3(a) shows the reconstructed image without correction for field inhomogeneities. Because of the fieldmap and gradient strength and the long readout time, there are significant geometric artifacts along with signal loss. Fig. 3(b) shows the reconstructed image when field inhomogeneities were corrected using the true fieldmap, but the through-plane gradients were ignored. In this reconstruction there are no geometric artifacts caused by field inhomogeneity, but there is significant signal loss due to the fieldmap gradients. Fig. 3(c) shows the reconstructed image with correction for field inhomogeneities and through-plane gradients, using the initial, standard fieldmap estimate (Fig. 3(d)) and the resulting gradients. In this case the artifacts are reduced but not completely eliminated, there is also some residual signal loss, and the reconstruction quality is not close to the one achieved in the oracle reconstruction (Fig. 2(a)), where the true fieldmaps and through-plane gradients are used. This is

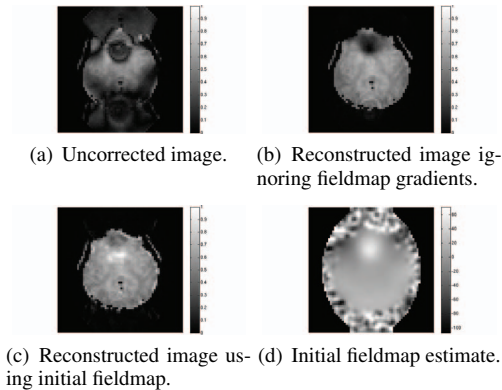


**Fig. 3.** Image and fieldmap reconstructions for one slice (slice 3 of sequence).

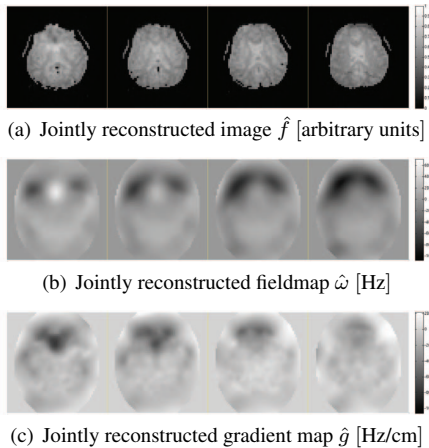


**Fig. 4.** Jointly reconstructed image, fieldmap and gradient map for 4 out of 20 slices. Slices 3, 8, 13 and 18 are shown from left to right.

also evident in terms of normalized RMS error, as seen in Table 1. Figs. 4(a), 4(b) and 4(c) show the jointly reconstructed images, fieldmaps and through-plane gradient maps that were reconstructed with our proposed method. In this case there are significantly reduced inhomogeneity artifacts and almost negligible signal loss in the reconstructed images; both the images, fieldmaps and gradients are of comparable quality to the oracle reconstructions (Figs. 2(a), 2(b) and 2(c)). This can also be seen in terms of RMS error in Table 1. As seen from these preliminary simulation results, the proposed method seems promising in performing efficient joint reconstruction of image and dynamic fieldmap in the presence of through-plane gradients.

## 5. DISCUSSION

This paper proposed an efficient method for joint estimation of dynamic images and fieldmaps compensating for through-plane gradient effects. The preliminary simulation results showed that high quality reconstruction can be achieved with this method, by using a more accurate signal model and fast approximations. Thus, this

	30dB	50dB	30dB	50dB
<b>Reconstructed images</b>	<b>NRMS in %</b>		<b>Max. Err. in %</b>	
uncorrected	49.4	49.1	99.7	99.9
using initial fieldmap	15.4	14.5	98.3	111.0
true fieldmap, no gradients	20.2	19.0	98.9	97.1
oracle (using true fieldmap)	9.1	4.9	41.4	29.5
joint estimation	10.2	7.3	67.6	74.9
<b>Reconstructed fieldmaps</b>	<b>RMS in Hz</b>		<b>Max. Err. in Hz</b>	
standard estimate	3.26	3.26	15.94	15.94
oracle (using true image)	0.27	0.24	2.36	2.29
joint estimation	1.33	1.40	11.78	13.86
<b>Reconstructed gradients</b>	<b>RMS in Hz/cm</b>		<b>Max. Err. in Hz/cm</b>	
standard estimate	17.01	17.01	150.32	150.32
oracle (using true image)	1.38	1.08	14.34	13.41
joint estimation	3.56	3.69	49.55	59.10

**Table 1.** Comparative table of RMS error of reconstruction methods, for all 20 slices.

method can be potentially useful in functional MRI, where dynamic fieldmap updates are desirable and through-plane gradient effects can cause significant image quality degradation. A disadvantage of this method, as in [2], is that non-standard single-shot trajectories seem to be required to achieve good reconstruction.

As a future step it would be interesting to investigate the benefits, in terms of quality of the reconstructed images, from incorporating in-plane fieldmap gradients in the signal model. Also, in this study, a 3D regularizer was used for fieldmap reconstruction, with promising results in terms of image quality. However, a more thorough study of its effects on the reconstructed images is required. Finally, to further evaluate the proposed method it is necessary to perform experiments using real data from phantom and human studies.

## 6. REFERENCES

- [1] B. P. Sutton, D. C. Noll, and J. A. Fessler, "Dynamic field map estimation using a spiral-in / spiral-out acquisition," *Mag. Res. Med.*, vol. 51, no. 6, pp. 1194–204, June 2004.
- [2] A. Matakos and J. A. Fessler, "Joint estimation of image and fieldmap in parallel MRI using single-shot acquisitions," in *Proc. IEEE Intl. Symp. Biomed. Imag.*, 2010, pp. 984–7.
- [3] D. B. Twieg and S. J. Reeves, "Basic properties of SS-PARSE parameter estimates," *IEEE Trans. Med. Imag.*, vol. 29, no. 5, pp. 1156–72, May 2010.
- [4] J. A. Fessler and D. C. Noll, "Model-based MR image reconstruction with compensation for through-plane field inhomogeneity," in *Proc. IEEE Intl. Symp. Biomed. Imag.*, 2007, pp. 920–3, Invited paper.
- [5] J. A. Fessler, S. Lee, V. T. Olafsson, H. R. Shi, and D. C. Noll, "Toeplitz-based iterative image reconstruction for MRI with correction for magnetic field inhomogeneity," *IEEE Trans. Sig. Proc.*, vol. 53, no. 9, pp. 3393–402, Sept. 2005.
- [6] V. T. Olafsson, D. C. Noll, and J. A. Fessler, "Fast joint reconstruction of dynamic  $R_2^*$  and field maps in functional MRI," *IEEE Trans. Med. Imag.*, vol. 27, no. 9, pp. 1177–88, Sept. 2008.
- [7] C. Yip, J. A. Fessler, and D. C. Noll, "Advanced three-dimensional tailored RF pulse for signal recovery in  $T_2^*$ -weighted functional magnetic resonance imaging," *Mag. Res. Med.*, vol. 56, no. 5, pp. 1050–9, Nov. 2006.
- [8] J. A. Fessler and W. L. Rogers, "Spatial resolution properties of penalized-likelihood image reconstruction methods: Space-invariant tomographs," *IEEE Trans. Im. Proc.*, vol. 5, no. 9, pp. 1346–58, Sept. 1996.

**Acknowledgment:** The authors acknowledge Doug Noll for discussions of fMRI imaging.